# Soft Matter

Accepted Manuscript






ROYAL SOCIETY OF CHEMISTRY

www.rsc.org/softmatter

ARTICLE TYPE www. rsc.org/xxxxxx | XXXXXXXX

# Internal stress drives slow glassy dynamics and quake-like behaviour in ionotropic pectin gels†

**Bradley W. Mansel§, Martin A.K. Williams¶**

***Received Xth XXXXXXXXXX 20XX, Accepted Xth XXXXXXXXX 20XX***
***First published on the web Xth XXXXXXXXXX 200X***
**DOI: 10.1039/b000000x**

Frustrated, out-of-equilibrium materials have been of considerable interest for some time and continue to be some of the least understood materials. Recent measurements have shown that many gelled biopolymer materials display slow dynamics on timescales greater than one second, that are not accessible with typical methods, and are characteristic of glassy trapped systems. In this study we have controlled the fine structure of the anionic polysaccharide pectin in order to construct a series of ionotropic gels having differing binding energies between the constituent chains, in an attempt to further understand the slow dynamical processes occurring. Using multi-speckle light scattering techniques it is shown that the slow dynamics observed in these gelled systems are stress-driven. As the binding lengths, and thus the binding energies, of the junction zones between the polymer chains in these networks increase the long-time dynamics initially slow, as might be expected, until a critical level of internal stress is reached upon which the dynamics increase significantly, with gentle creaking punctuated by localised stress-relieving quakes.

## 1 Introduction

Typically, colloidal glasses have been the canonical model for out-of-equilibrium materials that exhibit glassy dynamics and considerable amounts of underlying theory has been developed to describe their behaviour, such as mode coupling theory[1–3]. However, recent measurements on the dynamics of polysaccharide gels showing bi-modal dynamics, with slow modes reminiscent of those seen in other frustrated out of equilibrium systems highlight the breadth of soft materials exhibiting such behaviour[4–6]. It should perhaps not be surprising that such slow behaviour exists in polysaccharide gels, as syneresis, where the gel squeezes water from the network as it slowly pulls together, on time scales of hours or days has long been observed[7,8]. Typically in colloidal systems one seeks to understand the mechanism behind the slow internal dynamics: are they thermally driven or are they driven by internal-stresses built up as the system approaches the glass transition[9]? Here we investigate the interplay between the inter-polymer binding strength and the observed slow dynamics.

Recent experiments have highlighted many interesting phenomena regarding the slow dynamics in both pectin and alginate gels[4–6]. The slow dynamical processes occurring in pectin networks is an especially important topic, not only to understand the stability of gelled systems for controlled release in the food and pharmaceutical industries, but for the insights it may provide into how the plant cell wall, in which it is a major component, can elongate while maintaining its integrity, or perform directional motion in response to an external stimulus. In light of recent work we have designed three gels using three different pectin fine structures (the same monosaccharide composition of the chains, but different patterns of the cross linking moieties), to give differing binding strengths in a quest to predictably modify the slow dynamics.

Pectin, as found in the plant cell wall, is a complex heteropolysaccharide consisting of several domains, predominantly homo- and rhamno-galacturonan (RGI and RGII), the disposition of which is still a matter of debate to some extent[10]. It is clear however that the homogalacturonan (HG) backbone is connected through alpha 1-4 linkages and that it is the intermolecular association of this part of the polymer that is primarily responsible for pectin's ion-binding and gel forming capacity[11]. While RGI contains rhamnose residues, alternating with those of galacturonic acid, that act as sites of neutral sugar side chain attachment, these branches are often removed during commercial extraction procedures that are used to purify pectin and are subsequently not usually present in significant amounts in commercially available samples. In the plant cell pectin is biosynthesised as a weak acid with around 20 percent of the monomers in each homogalacturanan chain bearing naked carboxyl groups, with the remaining groups carrying a methyl ester. The ratio of methyl ester groups to

† Electronic Supplementary Information (ESI) available: Results of the PCI experiments are availible as .avi files. See DOI: 10.1039/b000000x/

*Fundamental Sciences, Massey University, Palmerston North, New Zealand. The MacDiarmid Institute for Advanced Materials and Nanotechnology, Wellington, New Zealand.*
§ *Email: bmansel@gmail.com*
¶ *Email: m.williams@massey.ac.nz*

acid groups is referred to as the degree of methyl esterification (DM) and can be modified using chemical or enzymatic procedures. Modifying the degree or pattern of methyl esterification can radically alter the gel forming abilities and mechanical properties of the subsequent gels formed. This makes pectin a particularly attractive biopolymer from which to create soft materials with designed mechanical properties.

Ionotropic pectin gels are formed when divalent ions, most commonly calcium, chelate a series of carboxyl groups on two different pectin chains, forming a bond between them. Two carboxyl groups binding a single calcium ion has a binding energy that is much lower than the thermal energy and hence cannot form a stable junction between chains. It has been calculated that between 8 and 15 consecutive bonds of this type are required to form a stable junction, and, as such, the distribution of the calcium chelating acid groups along a pectin chain is crucial in determining the gel-forming capacity. A higher degree of blockiness means that most of the acid groups are arranged in blocks along the chain, while a lower degree of blockiness means that most of the acid groups are more randomly distributed[12]. As described, the degree of blockiness plays a large role in determining the mechanical properties of a gel, as the number of binding groups in each junction defines the binding strength[13]. Indeed, a qualitative method used to categorise different pectins is to group them either as blocky pectins, forming stronger inter-chain junctions, or random pectins, forming weaker inter-chain associations. The number of ions available to form bonds is clearly another critical consideration in forming a gel: the number of ions relative to the number of pairs of carboxyl groups is typically defined as the $R$ value:

$$R = \frac{2\mathrm{Ca}^{2+}}{\mathrm{COO}^{-}} \quad (1)$$

with a value of one being where all the ions in the system have a pair of carboxyl groups potentially available to bind. The lowest R value that can form a gel depends on the degree of blockiness with typical R values for pectin gels being between 0.2 to 0.8, and a value greater than one meaning that there are more ions than binding sites, a situation that is not generally desirable.

Frustrated, out-of-equilibrium systems that display slow dynamics generally have similar dynamical behaviour: ultra slow relaxation that is often the result of internal stress and spatially and temporally heterogeneous dynamics that slow as the gel ages[14–16]. The understanding of these phenomena have been of considerable interest in recent years and they have been shown to exist in many soft systems. For this study we investigate these properties for 3 different ionotropic pectin gels assembled with calcium using the same R value, from polymers having the same DM but with different levels of blockiness, in a quest to modify the long-time dynamics. To verify that the different pectin samples studied did indeed form gels where the only predominant difference was the length of the inter-polymer junction-zone lengths we utilized Small-Angle X-ray scattering. Slow dynamical processes in these systems were studied using time-resolved multi-speckle dynamic light scattering techniques which offered simple and robust techniques to measure behaviour from non-ergodic samples, and achieve good statistics. Two different, albeit similar techniques, namely Photon Correlation Imaging (PCI) and multi-angle multi-speckle dynamic light scattering (MAMS DLS) were applied. PCI measures spatial information about the dynamics, which is particularly important for out-of-equilibrium systems, on length scales from around 50 $\mu m$ to 6 millimetres. MAMS DLS provides information on the mechanism driving the dynamics, by measuring how they scale with the scattering vector $q$. Where $q$ is related to the angle between the incident and scattered radiation, $\theta$, the refractive index of the medium, $n$ and the wavelength of the radiation $\lambda$ by: $q = 4\pi n \sin(\theta/2)/\lambda$. For out-of-equilibrium soft materials at large length scales the characteristic decay time, $\tau_f$ of the slow mode generally scales with the scattering vector as a power law with an exponent of -1, $\tau_f \propto q^{-1}$, indicating stress driven dynamics. In contrast, for systems with negligible internal stress the dynamics have been found to scale with a power law of exponent -2, $\tau_f \propto q^{-2}$, indicating thermally driven dynamics. For polysaccharide gels in general there has been some debate about the mechanism driving the slow dynamics, with speculation that if interchain binding strengths are near that of thermal energy the dynamics could indeed be thermally, and not stress, driven[6].

## 2 Materials and methods

### 2.1 Materials

Three pectin samples with a known degree of methylesterification (DM) and de-esterification methodology (that controls the intramolecular pattern of charged residues) were used for this study, two of which were purchased from CP Kelco and the other modified from apple pectin. The two purchased samples had: a DM of 43 and a random intramolecular charge pattern (R40), and a DM of 40 and a blockwise de-esterification pattern (B40) respectively. The other sample was modified from an apple pectin sample that had a starting DM of 75 (Sigma), by reducing the DM to 40 (P40), using pectin methylesterase (PME) extracted from orange (Sigma), under ideal conditions to produce a very blocky sample. The polymer fine structure modification was performed by first dissolving dried apple pectin in ultra pure water (milliQ) to a final polymer concentration of 0.25 wt% and then adjusting the pH to 7 using 1N and 0.1N analytical grade sodium hydroxide together with a calibrated digital pH meter. A pH-monitored demethylesterification method was then carried out. The pH of the solution

was monitored, and held at 7 by slowly adding known volumes of 0.1N NaOH, to counteract the active PME enzyme liberating galacturonic acid groups on the polymer backbone from their methyl esters, until the DM was lowered to 40 %. The sample was then heated to 80 °C to denature the PME, frozen using liquid nitrogen and finally freeze dried for 24 hours to allow for the long term storage of the dried polymer.

Gels with a final polymer concentration of 1 wt% were formed from the different polymers using the well-studied controlled calcium release gelation method, that introduces calcium using the dissolution of initially insoluble calcium carbonate. Gels were formed by dissolving 30 mg of the dried pectin in 2.37 ml ultra pure water (MilliQ) by mixing the suspended pectin with a magnetic stirrer for approximately 6 hours, then heating the solution to 50 °C for less than 30 minutes to ensure complete dissolution. To initiate gelation 2.32 mg of calcium carbonate with a nominal diameter of one micron was suspended in a solution consisting of 8.25 mg of glucono-$\delta$-lactone (GDL) in 0.593 ml of ultra pure water. This gave a ration of calcium ions to GDL of 1:2 which ensured that the pH of the solution was unchanged. The calcium carbonate and GDL solution was quickly added, within the order of tens of seconds, and mixed through the pectin solution to make a homogeneous solution, that was initially turbid owing to the inclusion of the calcium carbonate particles. The final sample weight was 3 grams. For samples with added tracer particles, 0.505 micron diameter polystyrene particles (Polysciences) were added to the calcium carbonate suspension to make the final phase volume of spheres in the sample 0.0013 %. Samples were left for 12 hours to gel in a 1.5 mm diameter quartz glass capillary for small-angle x-ray scattering measurements, a 10 mm path length cylindrical cuvette for dynamic light scattering, or a 10 mm path length rectangular cuvette for photon correlation imaging. After gelation the samples without added tracers had an almost transparent appearance with a low turbidity.

### 2.2 Small-angle x-ray scattering.

SAXS measurements were performed at the Australian Synchrotron on the SAXS beamline[17], where samples were prepared in 1.5 mm quartz glass capillary tubes (purchased from Hampton Research or capillarytubes.co.uk) and irradiated with 11 keV ($\lambda = 1.127$ Å) radiation. For this high-flux undulator-beamline a slit was used to attenuate the beam and multiple 1 second exposures were averaged over in order to increase the signal to noise ratio. Scattered radiation was collected using a Dextrus Pilatus 1M detector with the detector positioned either at 7179 or 719 mm from the sample which corresponds to a scattering vector, $q$, of 0.001-1 $Å^{-1}$. The scattering vector is defined as: $q = 4\pi\lambda^{-1}\sin(\theta/2)$, where $\theta$ is the angle between incident and scattered radiation. Absolute scattering intensities were measured using water as a standard scatterer.

### 2.3 Multiple-angle multi-speckle photon correlation spectroscopy.

MAMS PCS was used to measure the dynamics at multiple angles simultaneously. A setup with four CMOS detectors (Basler AG, model no. acA2040-90um) positioned around a sample formed in a 10mm path length cylindrical cuvette was illuminated with $\lambda = 532$ nm wavelength light, emitted from a 300 mW ultra-low-noise diode-pumped solid state laser (Cobolt Samba). The scattering vector is calculated from the scattering angle and is defined as: $q = 4\pi n\lambda^{-1}\sin(\theta/2)$, where $n$ is the refractive index of the solvent. Laser light was attenuated using a neutral density (ND) filter which reduced the power to levels where a good signal to noise ratio was observed. We estimate the power at the sample to be less than 100 mW. The setup was mounted on a large-area rotation stage (Thorlabs, model RBB18A), for ease of detector alignment, which was then positioned on an air damped optical table (Photon Control). The sample to detector distance was modified to adjust the speckle size to approximately the size of one pixel. Measurements were performed after allowing the sample to equilibrate for at least one hour in the sealed, temperature regulated, laboratory, with no other activity present and surrounded by curtains to further minimise low frequency air vibrations. Data were collected and post processed using the MATLAB programming environment.

The formalism outlined by ref. Cipelletti *et al.*[18] was used in the analysis, with the time resolved degree of correlation defined as:

$$c_I(t,\tau) = \frac{\langle I_p(t) I_p(t+\tau)\rangle_p}{\langle I_p(t)\rangle_p \langle I_p(t+\tau)\rangle_p} - 1 \qquad (2)$$

where $I_p(t)$ is the intensity recorded at the p$^{\text{th}}$ pixel at time $t$ and $\tau$ is the time lag. To improve statistics $c_I$ is averaged over a period of time to give:

$$g_2(t_w,\tau) - 1 = \langle c_I(t,\tau)\rangle_{t_w \le t \le t_w + t_{av}} \qquad (3)$$

where $t_w$ is the time between making the sample and performing the measurement. In addition

$$\chi(\tau) = \langle c_I(t,\tau)^2\rangle_t - \langle c_I(t,\tau)\rangle_t^2 \qquad (4)$$

where $\chi(\tau)$ is the variance of the correlation function, which is similar to the dynamical susceptibility as is often calculated in numerical work[19].

### 2.4 Photon correlation imaging.

PCI measurements were performed using the laser and ND filter as described above, although, for these experiments the

2mm diameter beam (at sample) was sent through a beam expander consisting of a pair of plano-cylindrical lenses to expand the beam into a vertical sheet with a height of 10mm. This line collimated beam was used to illuminate the sample which was gelled in a 10mm path length square cuvette (Hellma-Analytics) and scattered light was collected at an angle of 90° using a zoom lens (thorlabs, MVL7000) with internal aperture and a CMOS camera (Pixelink PL-B741) with a resolution of 1280 by 1024 pixels. The imaged area was 6.40 mm wide by 5.12 mm high, and each pixel at the detector corresponded to 5 $\mu m$ in real space. Data was collected then post processed using the MATLAB environment.

## 3 Results

### 3.1 Gel Structure

Measurements using SAXS, carried out to resolve and compare the structure of the three gels, all showed scattering profiles characterised by three different power law regimes, clearly indicated by the different slopes of these regions on a log-log plot. Broadly speaking, such plots reveal: in the low q region, a slope of -2.9; in the intermediate q regime a slope of -1; and at the highest accessible q values a slope of -3 (tending towards -4 for the P40 sample), although this is limited by the instrument background (figure 1). The low q results indicate highly clustered arrangements of the polymers in space. The intermediate and high q regimes display the scattering from the singular subunits, in this case a slope of around -1 indicating rod like entities compose the polymer network. The high q slope of -3 is consistent with the scattering from a rough surface fractal, as the interrogated length-scale becomes smaller than the diameter of the network strands. A model, in the form of a fractal structure factor with cylinder form factor was chosen to fit all three regimes simultaneously and is shown in figure 1 as solid black lines. The model accounts well for the scattering at the low and intermediate q regimes although it does not account for the rough surface fractal, represented by a slope of -3 in the high q regime. A model based on a rough cylinder form factor could be used, but is beyond the scope of this work. Using the standard scattering formalism, the measured intensity can be decomposed into three parts, a form factor, $P(q)$, which describes the form of the individual scatterers, a structure factor, $S(q)$, which describes the assembly of individual scatterers and a parameter $\Delta\rho$ which describes how strongly such a system should scatter and is related to the difference in electron density between the solvent and scatterer. A final parameter $n$ describes the number of scatterers in a volume, and these parameters are related by:

$$I(q) = n(\Delta\rho)^2 P(q) S(q) \quad (5)$$

For our system a cylinder form factor fitted the scattering profile well, as one would expect for rigid calcium-pectin junction zones. It contains a length, $L$ and radius, $r$ and is given by[20]:

$$P(q) = \int_0^{\pi/2} \left[ 2\frac{\sin(qL\cos(\alpha)/2)}{(qL\cos(\alpha)/2)} \frac{J_1(qr\sin(\alpha))}{(qr\sin(\alpha))} \right]^2 \sin\alpha d\alpha \quad (6)$$

where $J_1$ is the Bessel function of the first kind. The fractal structure factor is described by three parameters, $r_0$ describes the smallest length scale where the scattering becomes self similar, $D$ the fractal dimension and $\xi$ is the correlation length which describes a Guinier type behaviour at low $q$[21]:

$$S(q) = 1 + \frac{1}{(Qr_0)^D} \frac{D\Gamma(D-1)}{1+1/(q^2\xi^2)^{(d-1)/2}} \times \sin[(D-1)\tan^{-1}(q\xi)] \quad (7)$$

For the gels shown here, no Guinier type behaviour was seen and $\xi$ was set to a value larger than the lowest $q$. It can in any case be clearly seen that the three differ-

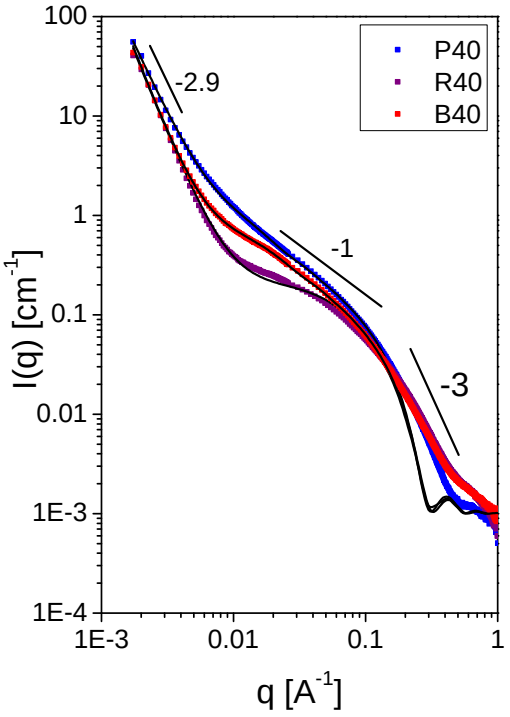


**Fig. 1** Small-angle x-ray scattering log-log plot showing the intensity (I) measured on an absolute scale as a function of scattering vector (q) for the three different gels. Small square symbols are the measured results and the solid lines are fits to a fractal structure factor with cylinder form factor model as described in the text.

ent ionotropic pectin gels produced similar scattering profiles in which the main difference is seen in the intermediate regime, reflecting the length-scale of the rod-like subunits. The model fitting confirmed that, as hypothesised, gels made from pectins with blockier intramolecular charge distributions indeed form longer rod-shaped structures (calcium-chelating junction zones), see table 1. Furthermore there is little difference in the radius of these junction-zones or their arrangement in space. The SAXS structural analysis confirms therefore that changes in the long-time dynamics of these different gels might safely be attributed to changes in the junction-zone strengths, and concomitantly their binding energies, as opposed to changes in the overall network architecture.

**Table 1** Table showing fitted parameters for the model shown in figure 1.

| Parameter fitted | R40 | B40 | P40 |
|---|---|---|---|
| $r$ [Å] | $12 \pm 1$ | $11.8 \pm 0.7$ | $12.3 \pm 0.2$ |
| $L$ [Å] | $70 \pm 20$ | $238 \pm 4$ | $300 \pm 30$ |
| $D$ | $2.911 \pm 0.005$ | $2.9355 \pm 0.0006$ | $2.7 \pm 0.2$ |
| $r_0$ [Å] | $78 \pm 2$ | $112.4 \pm 0.3$ | $150 \pm 20$ |

### 3.2 Slow Dynamics

To investigate the internal network dynamics the gels were either seeded with 505 nm diameter polystyrene spheres (for the MAMS DLS), or studied as-is (for PCI). In MAMS DLS experiments the additional spheres provided strong scattering centres to reduce the possibility that different sized heterogeneities in the gel network might produce angle-dependent scattering and complicate the analysis. Figure 2 shows correlation data and fits to an exponential function of the form: $g_2 - 1 \propto \exp[-(t/\tau_f)^\beta]$ where $\beta$ acts to either stretch, or compress the exponential decay depending on if it is less than or greater than one. It can be seen that the dynamics from the R40 and B40 gels show good fits to compressed exponential functions with compressing factor, $\beta$, between 1.3-1.7, depending on the sample, (values that are commonly seen in other soft glassy systems). The results for the P40 sample, figure 2, however, did not show a (compressed or stretched) exponential decay in the correlation function: while periodically the P40 gel could be described by a smooth exponential decay, most often the dynamics were highly heterogeneous and showed non-exponential decay behaviour as is shown in 2. Similar non-exponential decay behaviour has been observed for alginate gels[6]. While the other two pectin gels investigated here also showed non-exponential decay behaviour on occasion they predominantly showed a compressed exponential decay in the average degree of correlation.

Commonly in soft solids one tries to understand the driving mechanism behind the measured dynamics, which can be either stress or thermally driven. This can be done by measuring how the characteristic time associated with the slow dynamics scales with the scattering vector, in a similar way to distinguishing between ballistic and diffusive motion by observing how the mean-square-displacement scales with time. For this study four different scattering vectors were used to investigate the dynamics. A plot of the characteristic time corresponding to the slow dynamics, $\tau_f$, against scattering vector is shown in figure 3. It can be seen that the characteristic time clearly scales with the scattering vector as a power law with an exponent close to 1 (and not to 2), indicating that even for the gel composed of the smallest junction lengths the dynamics are driven by internal stresses and not thermally activated fluctuations of the junction-zone integrity. This should not be too surprising as these structures can easily support their own weight: evidence that a majority of bonds are stronger than thermal fluctuations, so that they do not slowly creep and flow. For these gels, even in the R40 sample which appears to be significantly softer than the others, the slow dynamics cannot be controlled by the thermally activated breaking of the weakest bonds, but instead is governed by collective rearrangements of the structure driven by stronger longer junctions continuing to "zip up".

To gain further insights into these slow dynamical processes the time-resolved degree of correlation, $c_I$, has been plotted for the $q = 18.9\mu m^{-1}$ data shown in figures 2, for different lag times, as shown in figures 4, 5 and 6. This angle was chosen as it probes intermediate length scales compared to the other angles. The dynamics appear to be stochastic; there is some probability that the internal stresses will build up sufficiently to trigger a phase of heterogeneous dynamics. Dynamical processes in these gels appear to fall broadly into three different categories; 1) at the shortest time scales there are "quake-like" fluctuations that yield intermittent sudden spikes in the degree of correlation; 2) on time scales of around 1000 seconds larger longer-lasting fluctuations reminiscent of creaking are evident, and 3) a universal decrease in the degree of correlation is also evident, that stays constant in time, as the time lag increases. The spiking and fluctuations are heterogeneous dynamics, and appear to be features of high levels of internal stress. The gels can enter a period of this type of dynamics then revert back to a temporally homogeneous regime as shown for the B40 gel in figure 5 where at a time of around 2000 seconds the dynamics switch from temporally heterogeneous to homogeneous. Figure 6 shows that most commonly the high levels of internal stress in the P40 gel make it predominantly display temporally heterogeneous dynamics. It can also be seen in figures 4, 5 and 6 that the time resolved degrees of correlation, $c_I(\tau)$, appear to increase following the highest frequency of quake-like events. This appears to be evidence of the build up and subsequent release of internal stresses, where the slow, steady drop in correlation signifies prolonged periods in which many small

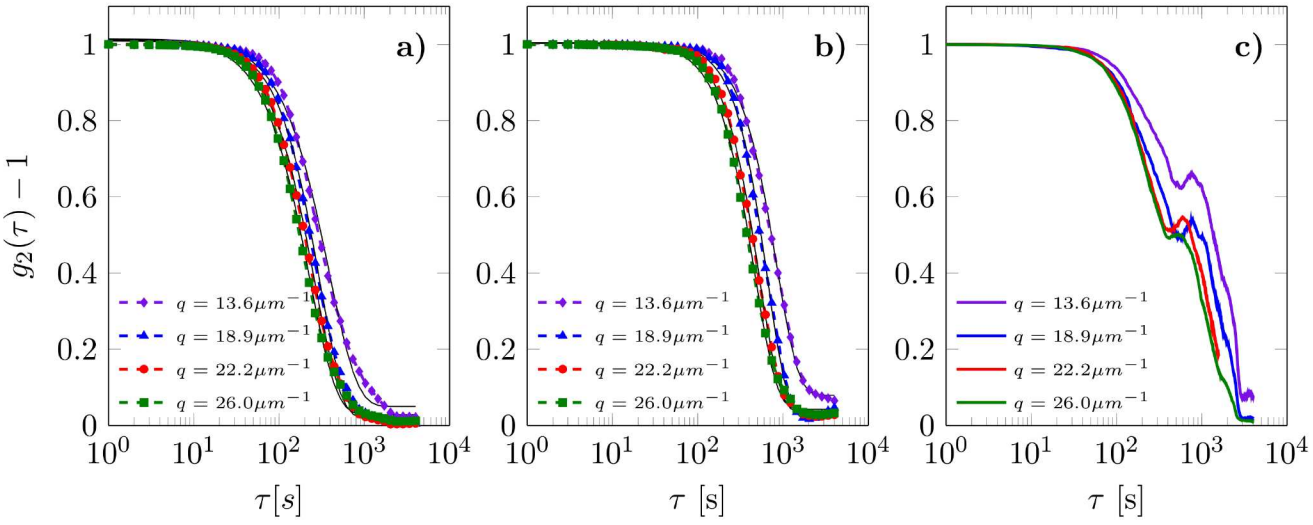


**Fig. 2** MAMS DLS for the three different gels seeded with 0.505 micron diameter polystyrene probe particles. Averaging has been performed over ten seconds, $t_{av} = 10s$. Solid lines represent compressed exponential fits with a compressing factor $\beta$ of between 1.3 and 1.7. figure a) is data recorded from the R40 sample, b) the B40 sample and c) the P40 sample.

dynamical events occur as the internal stress increases, that are punctuated by larger length-scale rapid quake-like events signifying a large release of the internal stress. Finally a drop in the number of small stress-building events events appears to be manifest following each series of quake-mediated relaxations, as shown by a gradual increase in $c_I(\tau)$. Plots of the variance of the degree of correlation,$\chi(\tau)$, figure 8 show a single peak corresponding to the time lag where there is maximum variation in the time resolved degree of correlation. The three gels show similar profiles, although the P40 sample displays significantly larger quake-like events at short time lags compared to the other gels.

While it has been proposed that the mechanism responsible for slow dynamics seen in calcium-assembled alginate gels could be the thermally-activated separation of junction-zones in contrast to the stress-driven dynamics observed herein, further experimental evidence supports the minimal involvement of the opening of unstressed junction-zones in these gels. Firstly, upon heating the gels to 80 °C there was no observed melting. Certainly for the R40 gel some softening of the gel was observed, but a solid, minimally-creeping structure seemed to be preserved. Upon heating the B40 gel, many small non-spherical "bubbles" became evident that are suggested to be the result of the higher temperature "annealing" whereupon larger junctions formed at the expense of shorter ones, thus increasing the internal stress to such high levels that weaknesses in the gel structure alleviate internal stress and "bubbles" are formed as a result of micro-fractures. For the P40 gel, upon heating, as well as the formation of these micro-fractures the gel underwent significant levels of syneresis, in

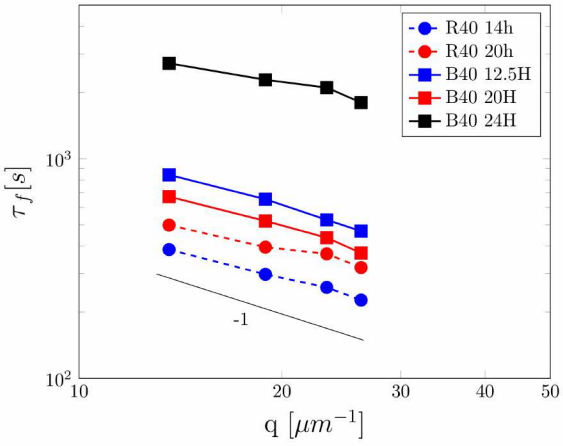


**Fig. 3** q vs. $\tau_f$ plots for the R40 and B40 pectin calcium gels at different ages. It can be seen that the characteristic times for the correlation functions scale with the scattering vector ($q$) with an exponent of approximately -1.

which the gel structure shrank in size to approximately half its pre-heated size. The non-melting and syneresis of these gels suggests that bond-breaking has little to do with the slow dynamics that we have observed at ambient temperatures, and instead that the continual rearrangements are driven not by thermal effects but by internal stresses resulting from larger junctions further associating. This hypothesis is in line with the results, that the polymer with the longest block length, that forms the longest junction zones, as confirmed by SAXs, does

not have the slowest dynamics, but on the contrary, the fastest most heterogeneous dynamics in many measurements.

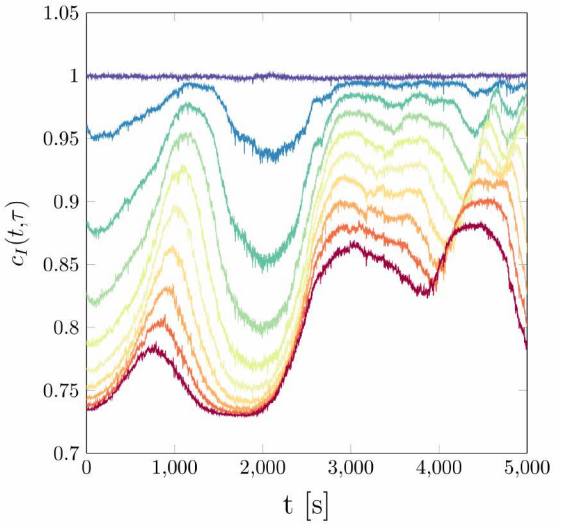


**Fig. 4** R40 time resolved correlation for 11 different lag times (from top to bottom, 1, 100, 200, 300, 400, 500, 600, 700, 800, 900 and 1000 seconds). The plot reveals a host of time scales over which the decorrelation of light occurs characteristic of heterogeneous dynamics.

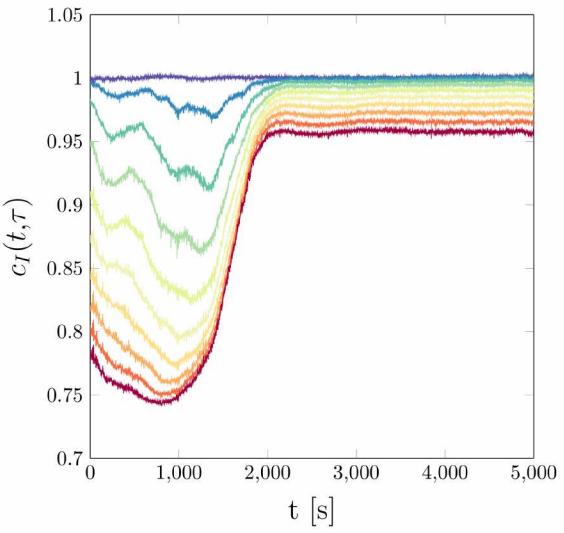


**Fig. 5** B40 time resolved correlation for 11 different lag times (from top to bottom, 1, 100, 200, 300, 400, 500, 600, 700, 800, 900 and 1000 seconds). This plot reveals that this sample undergoes a phase of temporally homogeneous dynamics where the correlation function has a flat response in time but decreases as the lag time increases.

Finally, the spatial extent of the correlations in the dynamics

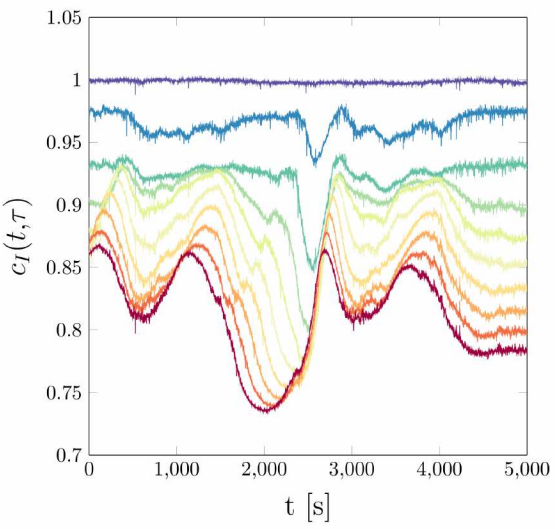


**Fig. 6** P40 time resolved correlation for 10 different lag times (from top to bottom, 1, 100, 200, 300, 400, 500, 600, 700, 800, 900 and 1000 seconds). It can be seen that the decorrelation of light evolves in a similar manner to the other gels, although some larger quake like events are present.

is investigated using photon-correlation imaging (PCI). PCI is a technique that spatially maps the decorrelation of light using a lens with an aperture to spatially filter and image the speckle pattern onto a CMOS detector (figure 7). For the set-up used during this study each pixel represents 5 $\mu m$ at the imaging plane, as described in the experimental section. To improve the signal to noise ratio, each pixel shown in figure 7 is a 10x10 pixel average of the recorded scattering image, corresponding to 50 $\mu m$ in the imaging plane. The colour in the false colour images corresponds to the value of the correlation function (dark red = 1, dark blue =0). It can be seen in figure 7 that the dynamics are spatially heterogeneous and the dynamics show, as has previously been documented in other soft systems, ultra long-range spatial correlations [19]. The ultra long-range correlation is an interesting phenomenon that has been reported to be a feature of enthalpic elasticity, which would be consistent with the SAXS structural analysis, which suggests the network is formed by rigid, rod like entities [19]. Little difference is seen between the three samples, but it should be noted that once again the sample constructed from the most blocky fine structure, that possesses the longest most thermally-stable junction zones shows the most varied dynamics (Movies Available On-Line)†.

### 3.3 Ageing

As is seen in other soft systems that display slow dynamical processes these pectin gels show dynamics that on average

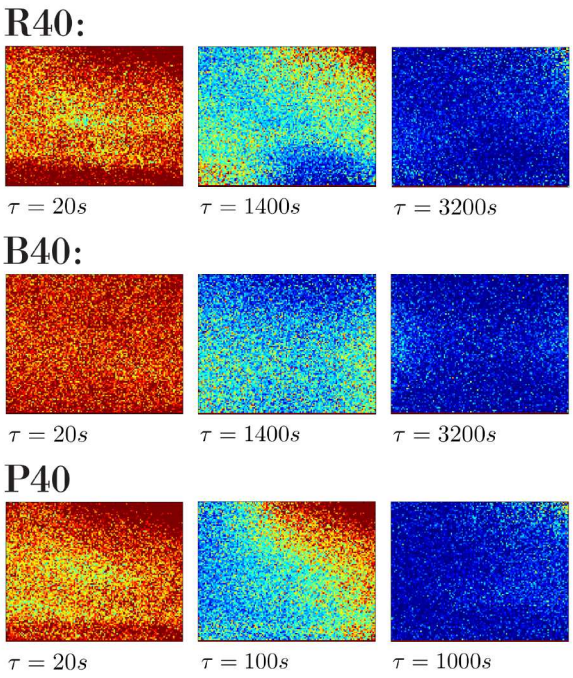


**Fig. 7** Photon-correlation images of the three different gels at different times. The colour in the false colour images corresponds to the value of the correlation function (dark red = 1, dark blue =0). One pixel corresponds to a measurement of the decorrelation averaged across an area of ten by ten pixels, or spatially $50 \times 50 \mu m$ corresponding to an area in the imaging plane of 6.40 mm wide by 5.12 mm high. The three gels show similar spatially resolved dynamics, although the P40 sample showed significantly faster dynamics during this measurement where the light was decorrelated after approximately 1000 seconds. It can also be seen that the gels have large scale spatial heterogeneities of the order of many millimetres.

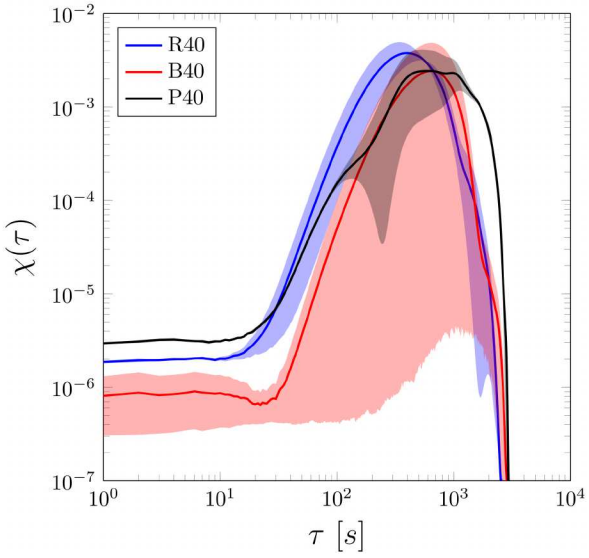


**Fig. 8** The variance of the time resolved dynamics for the three gels calculated with an average of $t_{av} = 3000s$ and an average over the two consecutive 3000s time periods shown in figures: 4, 5, 6. Shaded regions represent error estimations from the difference between the two 3000s time periods. The size of the fluctuations are similar as expected from the time resolved dynamics shown in figures 4, 5, 6, although it can be seen that at short times the P40 sample shows larger quake-like events compared to the other two gels. It can also be seen in fig. 5 that there is a period of homogeneous dynamics, this is reflected in the large error in the B40 data.

slow as the system ages. However, this ageing process is not at all linear. The relaxation processes occurring often appear to become jammed, and build internal stresses, the release of which causes the slowing of the dynamics to be punctuated by rapid quake-like fluctuations that are spatially heterogeneous but sweep over large distances in a correlated manner. As these systems go through such stochastic phases the dynamics are found to be highly temporally heterogeneous and exhibit correlation functions that have complicated non-exponential forms which may even increase before the correlation eventually decays to zero.

## 4 Conclusions

Three ionotropic gels of the polysaccharide pectin were assembled with calcium, using polymers that contained the same number of charged residues, but with different intramolecular distributions. As successful calcium-binding, which bridges chains and is the molecular process underlying successful network formation, requires a contiguous stretch of the charged galacturonic acid residues, the blockiness or otherwise of the pattern of charged groups along the backbone can be expected to be a crucial factor in gel formation. SAXS studies elucidated the calcium-mediated junction-zone lengths of the three gels created, and confirmed that using polymers with more blocky intramolecular charge distributions indeed provides longer inter-chain binding regions that can form longer, more thermally stable, junctions. However, rather than increasing the stability of the networks, if the junction-zone length is significantly increased, the internal dynamics can become driven by increasing internal stresses and become faster and more temporally heterogeneous. Imaging the dynamics, using PCI, showed that there are long range correlations in the dynamics, over several millimetres, many orders of magnitude larger than the rod-like entities forming the gel or the solid calcium carbonate particles that act as nuclei in the gel-formation process. Angle-resolved multi-speckle dynamic light scattering revealed that indeed the dynamics scale with a power law ex-

ponent of approximately -1 (and not -2) when changing the scattering vector, confirming that the dynamics in these systems are stress-driven for all gels measured. Increasing the junction zone length can increase the average characteristic time associated with these long timescale dynamics for intermediate blocklength pectin samples, but on the contrary, when very long junction zones can form, the dynamics often increase indicating that indeed long time internal network dynamics are not controlled by the thermally activated breakage of weaker junctions, but rather by their stress-induced disassembly driven by the propensity of larger junctions-zones to continue to assemble.

The authors acknowledge Dr. Allan Raudsepp for many discussions and valuable input to this work. Dr Che-Yi Chu and Prof. Hsin-Lung Chen for discussions about SAXS of biopolymer networks. Pablo Hernandez-Cerdan and Dr Stephen Keen for their critical reading of the manuscript. Funding for the SAXS section from the New Zealand Synchrotron group, the MacDiarmid institute for the PhD studentship (BWM) and Massey University for equipment Funding.

## References

1 E. R. Weeks, J. C. Crocker, A. C. Levitt, A. Schofield and D. A. Weitz, *Science*, 2000, **287**, 627–631.
2 W. Gtze, *Journal of Physics: Condensed Matter*, 1999, **11**, A1–A45.
3 W. Kob and H. C. Andersen, *Transport Theory and Statistical Physics*, 1995, **24**, 1179–1198.
4 E. Secchi, T. Roversi, S. Buzzaccaro, L. Piazza and R. Piazza, *Soft Matter*, 2013, **9**, 3931–3944.
5 E. Secchi, F. Munarin, M. D. Alaimo, S. Bosisio, S. Buzzaccaro, G. Ciccarella, V. Vergaro, P. Petrini and R. Piazza, *Journal of Physics: Condensed Matter*, 2014, **26**, 464106.
6 D. Larobina and L. Cipelletti, *Soft Matter*, 2013, **9**, 10005–10015.
7 D. Rees, *Advances in Carbohydrate Chemistry and Biochemistry*, Elsevier, 1969, vol. 24, pp. 267–332.
8 M. Kunitz, *The Journal of General Physiology*, 1928, **12**, 289–312.
9 L. Cipelletti and L. Ramos, *Journal of Physics: Condensed Matter*, 2005, **17**, R253–R285.
10 J.-P. Vincken, H. A. Schols, R. J. F. J. Oomen, M. C. McCann, P. Ulvskov, A. G. J. Voragen and R. G. F. Visser, *Plant Physiology*, 2003, **132**, 1781–1789.
11 D. A. Powell, E. R. Morris, M. J. Gidley and D. A. Rees, *Journal of Molecular Biology*, 1982, **155**, 517–531.
12 P. J. Daas, K. Meyer-Hansen, H. A. Schols, G. A. De Ruiter and A. G. Voragen, *Carbohydrate Research*, 1999, **318**, 135–145.
13 A. Strm, P. Ribelles, L. Lundin, I. Norton, E. R. Morris and M. A. K. Williams, *Biomacromolecules*, 2007, **8**, 2668–2674.
14 R. E. Courtland and E. R. Weeks, *Journal of Physics: Condensed Matter*, 2003, **15**, S359–S365.
15 C. Brito and M. Wyart, *Journal of Statistical Mechanics: Theory and Experiment*, 2007, **2007**, L08003–L08003.
16 L. Cipelletti, L. Ramos, S. Manley, E. Pitard, D. A. Weitz, E. E. Pashkovski and M. Johansson, *Faraday Discussions*, 2003, **123**, 237–251.
17 N. M. Kirby, S. T. Mudie, A. M. Hawley, D. J. Cookson, H. D. T. Mertens, N. Cowieson and V. Samardzic-Boban, *Journal of Applied Crystallography*, 2013, **46**, 1670–1680.
18 L. Cipelletti, H. Bissig, V. Trappe, P. Ballesta and S. Mazoyer, *Journal of Physics: Condensed Matter*, 2003, **15**, S257.
19 S. Maccarrone, G. Brambilla, O. Pravaz, A. Duri, M. Ciccotti, J.-M. Fromental, E. Pashkovski, A. Lips, D. Sessoms, V. Trappe and L. Cipelletti, *Soft Matter*, 2010, **6**, 5514.
20 A. Guimer and G. Fournet, *Small angle scattering of X-rays*.
21 J. Teixeira, *Journal of Applied Crystallography*, 1988, **21**, 781–785.